Contents lists available at ScienceDirect

# Scripta Materialia

journal homepage: www.elsevier.com/locate/scriptamat



# Grain boundary evolution of highly nanotwinned alloys: Effect of initial twinned microstructure



Joel A. Bahena<sup>a</sup>, Theresa Juarez<sup>a</sup>, Leonardo Velasco<sup>b</sup>, Andrea M. Hodge <sup>a,c,\*</sup>

- <sup>a</sup> Department of Aerospace and Mechanical Engineering, University of Southern California, Los Angeles, CA 90089, USA
- b Institute of Nanotechnology, Karlsruhe Institute of Technology, Hermann-von-Helmholtz-Platz 1, 76344 Eggenstein-Leopoldshafen, Germany
- <sup>c</sup> Department of Chemical Engineering and Materials Science, University of Southern California, 925 Bloom Walk, HED 216, Los Angeles, CA 90089, United States

#### ARTICLE INFO

Article history: Received 28 June 2020 Revised 16 August 2020 Accepted 18 August 2020

Keywords: Twinning Microstructural evolution Grain growth Nanostructured materials

#### ABSTRACT

The effects of initial twinned microstructure on the grain growth behavior of four sputtered nanotwinned copper alloys were compared. As-deposited films were characterized by transmission electron microscopy and the microstructural evolution of the annealed samples was investigated through electron backscatter diffraction. Texture showed a pronounced effect, where films with strong {111} textures exhibited abnormal grain growth that was not observed in a randomly textured film. Additionally, the stability induced by twin boundaries appears to be limited, as the excess energy generated by a large twin density could drive the early onset of abnormal grain growth and recrystallization.

© 2020 Acta Materialia Inc. Published by Elsevier Ltd. All rights reserved.

Nanotwins have emerged as a microstructural design feature that can improve several material properties in single element and alloyed metals, where these nanoscale twin boundaries exhibit lower grain boundary energy and can inhibit dislocation motion [1–3]. For instance, it has been demonstrated that nanotwinned (NT) Cu can display an increase in strength that follows a Hall-Petch relationship as the twin thickness ( $\lambda$ ) is reduced to a critical value of ~15 nm [4]. While the mechanical behavior of NT metals is largely attributed to the  $\lambda$ , recent studies comparing several NT Cu alloys have indicated that other microstructural features can also have significant roles [5,6]. Hence, a more comprehensive examination of the initial NT microstructure is needed, especially in terms of grain growth and thermal stability.

Previous studies have shown that NT metals are more thermally stable than nanocrystalline or ultra-fined grained counterparts as a function of twin boundaries pinning columnar grain boundaries and impeding grain boundary migration [7,8]. However, other studies suggested that a high density of twins is insufficient to stabilize the microstructure at elevated temperatures, requiring an investigation of the initial twinned microstructure [9–11]. To date, a comparison across similar NT microstructures has not been conducted especially since different synthesis methods can dictate characteristics (grain size, texture, twin density, residual stresses, etc) that impact thermal evolution. Although the role of these microstruc-

tural features is not well understood, it has been proposed that decreasing  $\lambda$  could improve thermal stability by increasing the number of triple junctions and constraining grain boundary motion [12]. Despite twin boundaries typically exhibiting an order of magnitude less energy than high angle grain boundaries, a large twin boundary density could increase the overall grain boundary energy and initiate the onset of grain growth at lower temperatures [7]. Reducing the grain size and/or grain width could have a similar affect and encourage a tendency towards grain coarsening, especially at the nanoscale [13]. Furthermore, experimental results point towards certain crystallographic textures and intrinsic residual stresses promoting grain coarsening and abnormal grain growth behavior in nanostructured materials [14,15]. Thus, there is potential that particular grain orientations and stored energy distributions could be more favorable in resisting grain boundary mobility.

In this letter, the influence of  $\lambda$ , grain width, texture, and intragranular orientation spread are evaluated to investigate the factors affecting grain growth in sputtered NT Cu alloys. Specifically, transmission electron microscopy (TEM) was used to characterize as-deposited films and the thermal microstructural evolution was analyzed through electron back scatter diffraction (EBSD). Overall, this study examines how the characteristics of an initial twinned microstructure can lead to the activation of distinct thermal processes and contribute to mitigating grain growth in NT metals.

Two sets of NT Cu alloy films with varying microstructural features were examined in this study and were synthesized by

<sup>\*</sup> Corresponding author.

E-mail address: ahodge@usc.edu (A.M. Hodge).

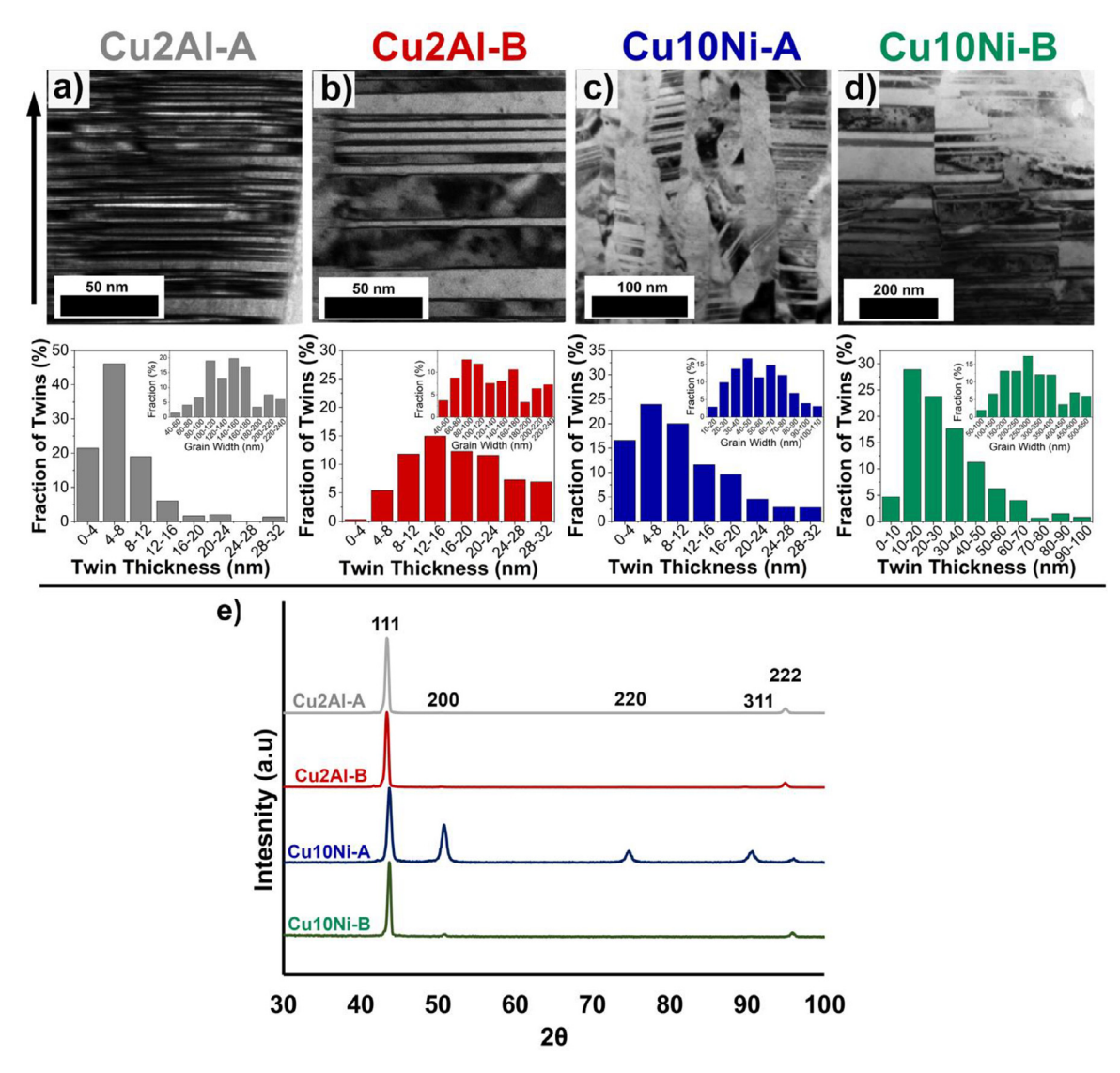


Fig. 1. Cross-sectional bright field TEM comparing as-sputtered (A) Cu2Al-A ( $\lambda$ =5 nm), (B) Cu2Al-B ( $\lambda$ =18 nm), (C) Cu10Ni-A ( $\lambda$ =13 nm), and (D) Cu10Ni-B ( $\lambda$ =31 nm); and (E) representative XRD scans of the NT alloys. The arrow to the left indicates the film growth direction.

magnetron sputtering. Samples deposited using a Cu-2wt.Al target are labeled Cu2Al-A ( $\lambda$ =5 nm) and Cu2Al-B ( $\lambda$ =18 nm) and have the same composition. Similarly, samples deposited using a Cu-10wt.%Ni target are labeled Cu10Ni-A ( $\lambda$ =13 nm) and Cu10Ni-B ( $\lambda$ =31 nm) and also have the same composition. The microstructure and  $\lambda$  of each film were tuned by altering the sputtering parameters based on procedures from Velasco et al [16]. A summary of the sputtering conditions can be found in the Supplementary Information. The film thicknesses ranged from 14-19  $\mu$ m, which was measured by an XP-2 stylus profilometer (AMBiOS). Electron transparent lamellae were prepared with a Fischione 1050 ion mill and were characterized via TEM using a JEM-2100F (JEOL) microscope. In addition, crystallographic information was obtained by performing X-ray diffractometry measurements using a Rigaku Ultima IV diffractometer. To investigate the microstructural evolution of the NT alloys at elevated temperatures, free-standing films were successively heat treated at temperatures of 200°C, 400°C, and 600°C for two hours in a vacuum ( $< 10^{-5}$  torr) tube furnace at a heating rate of 10°C/min. Top-surface EBSD scans of the films after each heat-treatment were captured using a JEOL-7001 SEM with an EDAX Hitari Detector and a FEI Helios G4 with an Oxford Symmetry Detector. EBSD datasets were analyzed with the MTEX software [17]. To complement the study, micro-hardness testing was performed using a Vickers tip with 10 g indents, totaling five indents for each sample.

A summary of the samples is displayed in Fig. 1, presenting representative cross-sectional TEM, grain width and  $\lambda$  distributions, and XRD patterns. The TEM micrographs at different magnifications, shown in the top portion of Fig. 1A-D, highlight key microstructural features for each film. All microstructures consisted of mostly vertical columnar grains containing a high-density of twin boundaries perpendicular to the growth direction, but Cu10Ni-A has several inclined twin boundaries. Below, the respective  $\lambda$  and grain width (inset) distributions are displayed for the four samples. These plots were obtained by measuring a minimum of 200 grains and 500 twins for each sample. Cu2Al-A, Cu2Al-B, Cu10Ni-A, and Cu10Ni-B have an average grain width of 140  $\pm$  40 nm, 130  $\pm$  70 nm, 50  $\pm$  20, and 260  $\pm$  130 and an average  $\lambda$  of 5 nm, 18 nm, 13 nm, and 31 nm, respectively. The XRD patterns in Fig. 1E, reveal a strong {111} texture for Cu2Al-A, Cu2Al-B, and Cu10Ni-B, which is common for sputtered NT FCC metals, while Cu10Ni-A exhibits a random texture.

The grain size evolution of each sample was evaluated by EBSD in the as-sputtered condition and after heat-treatments at 200°C,

**Table 1**Summary of Vickers hardness (HV) and grain size from top-surface EBSD of as-sputtered NT Cu alloys and after successive heat treatments at 200°C, 400°C, and 600°C.

	Cu2Al-A (λ=5 nm)		Cu2Al-B (λ=18 nm)		Cu10Ni-A (λ=13 nm)		Cu10Ni-B (λ=31 nm)	
	Hardness (HV)	Grain Size (nm)	Hardness (HV)	Grain Size (nm)	Hardness (HV)	Grain Size (nm)	Hardness (HV)	Grain Size (nm)
AS	$340\pm2$	130	$310 \pm 6$	140	$400 \pm 3$	50	$300 \pm 6$	250
200°C	$340\pm3$	140	$300 \pm 4$	150	$370 \pm 4$	120	$280\pm2$	270
400°C	$90 \pm 8$	1550	$210 \pm 5$	165	$350 \pm 2$	150	$250 \pm 4$	290
600°C	$90 \pm 3$	1580	$100 \pm 3$	5100	$170\pm2$	340	$80 \pm 1$	7800

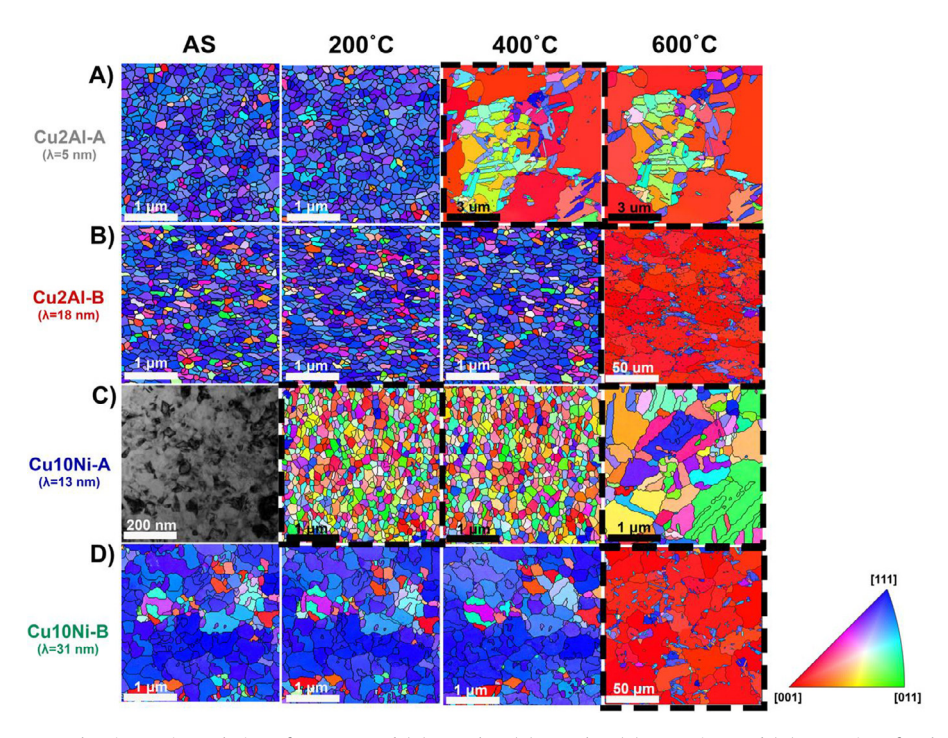
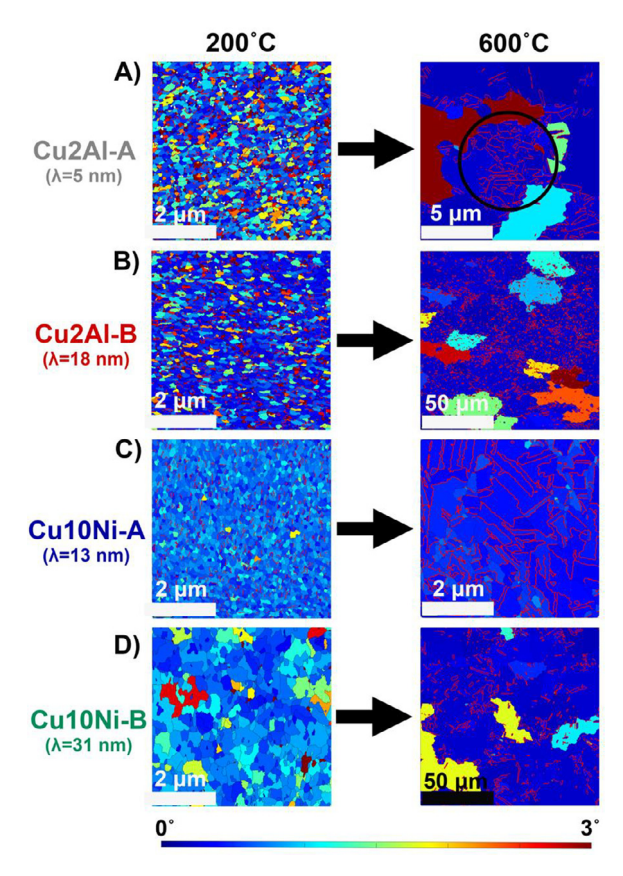


Fig. 2. Top surface EBSD IPF maps showing grain evolution of as-sputtered (A) Cu2Al-A, (B) Cu2Al-B, (C) Cu10Ni-A, and (D) Cu10Ni-B after heat treatments performed at 200°C, 400°C, and 600°C. Dashed boxes highlight instances of significant grain growth, note the changes in scale bar. The IPF triangle is shown to the right of the scans.

400°C, and 600°C for 2 hours, which is presented in Table 1. Based on XRD scans of the samples annealed at 600°C, provided in the Supplementary Information, the grain growth behavior of these films is not expected to be influenced by the formation of secondary phases or intermetallics. Additionally, Vickers micro-hardness was used as a complementary technique to analyze microstructural stability and provide insight to microstructural changes not detectable through top-surface characterization [10]. It should be noted that the EBSD measurements of the planar grain sizes of the as-sputtered films are consistent with the grain widths determined by cross-sectional TEM. The grain size data from Table 1 is complementary to Fig. 2, which displays the inverse pole figure (IPF) maps of the top-surface after each successive heat treatment performed near or at the same region. In addition, instances of significant grain growth during the thermal microstructural evolution are indicated by dashed boxes outlining scans in Fig. 2. Note that the ~50 nm grain size of Cu10Ni-A in the as-deposited film was not detectable by EBSD, therefore a planar-view TEM micrograph is substituted to illustrate the microstructure. Overall at 200°C few changes are observed for each microstructure except for Cu10Ni-A, where the grain size increased from ~50 nm to ~120 nm while maintaining a random texture. At 400°C, Cu2Al-A shows sudden grain growth with larger {100} grains consuming the majority of the microstructure, producing an average grain size of ~1550 nm and having large clusters comprised of randomly oriented grains dispersed throughout film. The remaining three samples do not display significant grain coarsening until 600°C where Cu2Al-B and Cu10Ni-B undergo similar abnormal grain growth as seen in Cu2Al-A at 400°C. with an average grain size for both films increasing to over 5000 nm. In contrast, Cu10Ni-A undergoes a second instance of coarsening at 600°C but retains a relatively fine grain size of ~350 nm and a random texture.

The evolution of hardness with increasing temperature closely correlates with the observed grain size changes. In the asdeposited state, the hardness values were all greater than 300 HV. with Cu10Ni-A exhibiting the highest hardness at 400 HV. The recorded values are comparable to those of previous NT Cu studies with similar grain widths [8]. At 200°C, Cu10Ni-A shows a minimal decrease in hardness, which would suggest retention of the nanotwinned structure despite this initial increase in grain size. Furthermore, at 400°C the hardness for Cu2Al-A drops below 100 HV corresponding with the observed abnormal grain growth. In addition, moderate drops in hardness for both Cu2Al-B and Cu10Ni-B are recorded despite no significant change in grain size, which could indicate the onset of detwinning and relaxation of residual stresses [9,18,19]. A significant decrease is observed at 600°C, at which abnormal grain growth occurs for both films. The hardness for Cu10Ni-A, even at 600°C, remains relatively high at 170 HV, reflecting a more thermally stable sample.

In addition to grain size and  $\lambda$ , microstructural heterogeneity has also been shown to influence grain growth behavior of NT materials [7, 9]. For instance, it has been previously reported that grain coarsening and recrystallization processes in NT Cu can



**Fig. 3.** Top surface EBSD maps showing the GOS distribution for samples annealed at  $200^{\circ}$ C and  $600^{\circ}$ C.  $\Sigma 3$  grain boundaries are outlined in red.

be selective depending on misorientation between adjacent grains [10]. Likewise, a heterogenous distribution of stored energy has been shown to activate distinct grain growth or recrystallization mechanisms in many coarse-grained alloys, which could provide more insight into the varied microstructural evolutions observed in this study [20-23]. In order to obtain a qualitative representation of the evolution of stored energy and insight into thermal processes occurring in these films, grain orientation spread (GOS) maps of the samples annealed at 200°C and 600°C are presented in Fig. 3. The GOS spread is colored from 0° to 3°, where studies have demonstrated that grains with larger orientation spreads (red) are expected to have higher stored energy [21]. Considering that not all as-sputtered samples were resolved by EBSD, 200°C was selected as the initial temperature for comparison purposes. At 200°C, the GOS maps indicate a relatively wide GOS distribution for both Cu2Al samples (Fig. 3A and B) as illustrated by the heterogenous collection of grains with small (low stored energy) and large (high stored energy) orientation spreads. Meanwhile, the GOS map for Cu10Ni-A (Fig. 3C) displays a mostly homogeneous distribution with relatively low spreads, whereas Cu10Ni-B (Fig. 3D) exhibits moderate heterogeneity. In terms of abnormal grain growth, grains with lower stored energy have a competitive advantage over those with higher stored energy [21], which could contribute to the formation of abnormally large grains in Cu2Al-A, Cu2Al-B, and Cu10Ni-B. As previously discussed, these three films exhibit strong {111} textures which points to a correlation between stored energy and the initial texture, as seen in other studies [24–26]. Upon annealing at 600°C, the overall GOS values decreased across all films, but several abnormally large grains retain relatively large orientation spreads, implying the microstructures have yet to reach a steady state [27]. In the case of Cu2Al-A, the clusters of randomly oriented grains are characterized (encircled) by large networks of annealing twins and low orientation spreads, which indicate recrystallization and the presence of twin related domains (TRDs) [28,29]. Cu10Ni-A also exhibits a large network of twins, but the lower initial orientation spreads and preserved random texture would suggest a strain induced boundary migration (SIBM) process rather than recrystallization [20,29]. Thus, it is likely that twin boundary network is a result of residual twins that were not annihilated during the grain growth process at elevated temperatures

Based on observations, the initial NT microstructure appears to have a pronounced effect on the grain growth behavior. Through comparing the different alloy pairs of the same composition, the influence of distinct microstructural features can be identified. Cu2Al-A and Cu2Al-B share similar microstructural characteristics, but the twin density is ~3 times greater for Cu2Al-A. It was shown that both samples exhibit some level of abnormal grain growth dominated by the formation of large {100} grains, but the onset occurs at 400°C for Cu2Al-A and at 600°C for Cu2Al-B. It is possible that an initial lower  $\lambda$  could initiate thermal process at lower temperatures due to the increase in excess energy associated with twin boundaries [7,9,10]. For example, in a previous study examining NT Ag ( $\lambda$ =10 nm), the calculated driving force of 1000 kJ/m<sup>3</sup>, was predicted to significantly contribute to the activation of abnormal grain growth [30]. In the case of Cu2Al-A and Cu2Al-B, similar calculation were performed assuming a twin boundary energy of 24 mJ/m<sup>2</sup> [31], which yields estimated driving force values of 4800 kJ/m<sup>3</sup> and 1333 kJ/m<sup>3</sup>, respectively. In addition, many of the twins observed for Cu2Al-A are slightly curved which would indicate the presence of highly mobile incoherent twin segments that could contribute to the observed early onset of recrystallization and abnormal grain growth [9]. The increased driving force is further highlighted by the presence of TRDs in select regions of the Cu2Al-A microstructure, which typically require a higher driving force to initiate when compared to abnormal grain growth [28]. Although the onset of grain growth in Cu2Al-A starts at a lower temperature, this does not necessarily result in a larger grain size, since there are always multiple mechanism present. For example, the formation of TRDs in Cu2Al-A impinge and restrict the growth of abnormally large grains that would otherwise consume higher stored energy regions, leading to a smaller grain size by a factor of ~3. However, these observations do indicate that a critical  $\lambda$  exists that can reduce thermal stability by driving the early onset of abnormal grain growth and recrystallization as shown for Cu2Al-A at

Further insight into the implications of initial grain size and texture is gained by extending observations to the grain growth behavior of Cu10Ni-A and Cu10Ni-B. In terms of these microstructural features, Cu10Ni-A has a grain size of ~50 nm with a random texture, while Cu10Ni-B has a grain size of ~250 nm and a strong {111} texture. The difference in texture can be attributed to the formation of inclined twins for Cu10Ni-A, which have shown to promote changes in columnar grain texture [32]. The effects of differing initial grain size is evident after the 200°C heat treatment, where Cu10Ni-B remains microstructurally similar, but grain growth is observed for Cu10Ni-A as a function of the ~5-fold increase in grain boundary density [13]. Despite the early onset of coarsening and the larger driving force associated with a higher grain boundary energy, at 600°C, Cu10Ni-A retains a relatively small grain size. This discrepancy in grain growth behavior appears to be influenced by the texture evolution of each film, where EBSD revealed that Cu10Ni-A preserves a random texture and Cu10Ni-B exhibits a {111}-to-{100} texture shift. Although a strong {111} texture can provide improved thermal stability owing to a large fraction of low angle grain boundaries [7,8,33], dispersed {100} grains present in Cu10Ni-B introduce high angle grain boundaries with increased mobilities that facilitate rapid growth at elevated

temperatures [27,34]. In contrast, the random texture of Cu10Ni-A promotes a wider grain boundary character distribution that diminishes the growth advantage for pre-existing {100} grains and prompts a more gradual grain growth behavior [34,35]. Thus, from our observations across all NT samples, initial film texture appears to be the dominant microstructural characteristic for resisting abnormal grain growth.

In summary, the thermal evolution of four sputtered NT Cu alloys have been compared to understand the effect of initial twinned microstructure on grain growth behavior at elevated temperatures. Texture induced by inclined twin boundaries appears to be a crucial factor in facilitating grain growth behavior, where NT films with a strong {111} texture demonstrated the tendency to form abnormally large {100} grains and the film with a random texture (Cu10Ni-A) demonstrated a stepwise growth behavior. Additionally, previous studies have theorized that a large twin density can stabilize NT metals, but the present work indicates that there is a threshold to this stabilizing effect, where a smaller  $\lambda$  can drive the early onset of abnormal grain growth and recrystallization. Overall, the findings from this study provide insight into the role of the specific microstructural characteristic that can be leveraged to design more stable NT systems.

## **Declaration of Competing Interest**

The authors declare that they have no known competing financial interests or personal relationships that could have appeared to influence the work reported in this paper.

#### Acknowledgements

This work was supported by the National Science Foundation under Grant DMR-1709771 and the Office of Naval Research under grant N00014-18-1-2617. We acknowledge the Core Center of Excellence in Nano Imaging (CNI) at the University of Southern California for the characterization facilities.

### Supplementary materials

Supplementary material associated with this article can be found, in the online version, at doi:10.1016/j.scriptamat.2020.08. 024.

#### References

- [1] Y. Zhao, I.C. Cheng, M.E. Kassner, A.M. Hodge, Acta Mater. 67 (2014) 181-188.
- [2] G.D. Sim, J.A. Krogstad, K.M. Reddy, K.Y. Xie, G.M. Valentino, T.P. Weihs, K.J. Hemker, Sci. Adv. 3 (6) (2017) e1700685.
- [3] J.R. Greer, Nat. Mater. 12 (8) (2013) 689-690.
- [4] L. Lu, X. Chen, X. Huang, K. Lu, Science 323 (5914) (2009) 607-610.
- [5] N.M. Heckman, L. Velasco, A.M. Hodge, Adv. Eng. Mater. 18 (6) (2016) 918-922.
- [6] N.M. Heckman, L. Velasco, A.M. Hodge, MRS Commun. 7 (2) (2017) 253–258. [7] Y. Zhao, T.A. Furnish, M.E. Kassner, A.M. Hodge, J. Mater. Res. 27 (24) (2012)
- [7] Y. Zhao, T.A. Furnish, M.E. Kassner, A.M. Hodge, J. Mater. Res. 27 (24) (2012) 3049–3057.
- [8] X. Zhang, A. Misra, Scripta Mater. 66 (11) (2012) 860-865.
- [9] T. LaGrange, B.W. Reed, M. Wall, J. Mason, T. Barbee, M. Kumar, Appl. Phys. Lett. 102 (1) (2013) 011905.
- [10] R. Niu, K. Han, Y.F. Su, T. Besara, T.M. Siegrist, X. Zuo, Sci. Rep. 6 (2016) 31410.
- [11] Y.M. Wang, F. Sansoz, T. LaGrange, R.T. Ott, J. Marian, T.W. Barbee Jr., A.V. Hamza, Nat. Mater. 12 (8) (2013) 697–702.
- [12] C. Saldana, T.G. Murthy, M.R. Shankar, E.A. Stach, S. Chandrasekar, Appl. Phys. Lett. 94 (2) (2009) 021910.
- [13] H.R. Peng, M.M. Gong, Y.Z. Chen, F. Liu, Int. Mater. Rev. 62 (6) (2017) 303-333.
- [14] L. Cao, A. Sengupta, D. Pantuso, M. Koslowski, Model. Simul. Mater. Sci. Eng. 25 (7) (2017) 075004.
- [15] P. Sonnweber-Ribic, P.A. Gruber, G. Dehm, H.P. Strunk, E. Arzt, Acta Mater. 60 (5) (2012) 2397–2406.
- [16] L. Velasco, A.M. Hodge, Acta Mater. 109 (2016) 142-150.
- [17] F. Bachmann, R. Hielscher, P.E. Jupp, W. Pantleon, H. Schaeben, E. Wegert, J. Appl. Crystallogr. 43 (6) (2010) 1338–1355.
- [18] D. Bufford, H. Wang, X. Zhang, J. Mater. Res. 28 (13) (2013) 1729–1739.
- [19] J. Wang, N. Li, O. Anderoglu, X. Zhang, A. Misra, J.Y. Huang, J.P. Hirth, Acta Mater. 58 (6) (2010) 2262–2270.
- [20] A. Nye, A.C. Leff, C.M. Barr, M.L. Taheri, Scripta Mater. 146 (2018) 308-311.
- [21] T.A. Bennett, P.N. Kalu, A.D. Rollett, Microsc. Microanal. 17 (3) (2011) 362-367.
- [22] T.S. Prithiv, P. Bhuyan, S.K. Pradhan, V. Subramanya Sarma, S. Mandal, Acta Mater. 146 (2018) 187–201.
- [23] J.A. Bahena, N.M. Heckman, C.M. Barr, K. Hattar, B.L. Boyce, A.M. Hodge, Acta Mater. 195 (2020) 132–140.
- [24] G. Abadias, E. Chason, J. Keckes, M. Sebastiani, G.B. Thompson, E. Barthel, G.L. Doll, C.E. Murray, C.H. Stoessel, L. Martinu, J. Vac. Sci. Technol. A 36 (2) (2018) 020801.
- [25] S. Birosca, Metall. Mater. Trans. A 50 (2) (2019) 534-539.
- [26] M. Wang, R. Xin, B. Wang, Q. Liu, Mater. Sci. Eng. 528 (6) (2011) 2941–2951.
- [27] F.J. Humphreys, M. Hatherly, Recrystallization and Related Annealing Phenomena, Elsevier, 2012.
- [28] C.M. Barr, A.C. Leff, R.W. Demott, R.D. Doherty, M.L. Taheri, Acta Mater. 144 (2018) 281–291.
- [29] D.B. Bober, J. Lind, R.P. Mulay, T.J. Rupert, M. Kumar, Acta Mater. 129 (2017) 500–509.
- [30] E.A. Ellis, M. Chmielus, M.-T. Lin, H. Joress, K. Visser, A. Woll, R.P. Vinci, W.L. Brown, S.P. Baker, Acta Mater. 105 (2016) 495–504.
- [31] L.E. Murr, Interfacial Phenomena in Metals and Alloys, Addison-Wesley Publishing Company, United States, 1975.
- [32] L. Velasco, A.M. Hodge, Mater. Sci. Eng. 687 (2017) 93-98.
- [33] H. Ma, Y. Zou, A.S. Sologubenko, R. Spolenak, Acta Mater. 98 (2015) 17-28.
- [34] N. Moelans, F. Spaepen, P. Wollants, Philoso. Mag. 90 (1-4) (2010) 501-523.
- [35] E.A. Holm, M.A. Miodownik, A.D. Rollett, Acta Mater. 51 (9) (2003) 2701–2716.